Dynamics of shear stress reversals and riffle maintenance in a gravel-bed stream

David Gaeuman, Senior Geomorphologist, Yurok Tribe Fisheries Dept., Weaverville, CA, dgaeuman@yuroktribe.nsn.us

Kyle DeJuilio, Senior Biologist, Yurok Tribe Fisheries Dept., Weaverville, CA, kdejuilio@yuroktribe.nsn.us

D. Nate Bradley, Geomorphologist, U.S Bureau of Reclamation, Denver, CO, dnbradley@usbr.gov

Introduction

Pool-riffle sequences are ubiquitous features of alluvial stream, especially streams with gravel-to-cobble substrates (Leopold et al. 1964; Knighton 1998). These structural elements contribute to habitat diversity that underlies aquatic ecosystem integrity (Hawkins et al. 1993; Jowett 1993). The prevalence and importance of pool-riffle morphology has generated considerable interest in the processes that create and maintain them.

Riffles are, by definition, places where bedload is deposited during flow events that mobilize the stream bed. It is therefore necessary that shear stresses (τ) at riffle locations be small enough during floods for bedload to accumulate, even though τ at riffles tends to be relatively large during baseflow periods. Keller (1971) was among the first to explicitly discuss this aspect of riffle maintenance and proposed that the location of the highest flow velocities shifts from riffles to pools as discharge increases to levels that mobilize the stream bed. This "velocity reversal" hypothesis was subsequently modified to recognize the potential for reversals in the locations of the higher τ during floods (Lisle 1979), or at least an equalization of τ at riffle and pool locations (Carling 1991). More recent studies appear to confirm that consideration of flow velocity alone cannot explain the distribution of pools and riffles. MacVicar and Roy (2007), for example, suggest that greater turbulent kinetic energy related to the transition to greater depth boosts transport capacity at the entrance to pools during floods even though mean flow velocities may remain relatively low, whereas the transitions to shallower flow over riffles generate higher near-bed velocities that route bedload around the pools. Others have extended the idea of velocity or τ reversals to include factors such as local flow divergence and convergence (Cao et al. 2003; MacWilliams et al. 2006), changes in downstream backwater conditions (Pasternack et al. 2008), and lateral shifts in the position of maximum τ or lanes of bedload transport (Wilkinson et al. 2004; Milan 2013).

The lack of consensus on precisely how pool-riffle morphology arises may be due to the diversity in the configurations of pools and riffles, as well as to differences in the spatial scales and densities at which hydraulic variables are measured in different studies (MacVicar and Roy 2007; Thompson 2010). Pools and riffles display a wide range of spatial scales, detailed morphologies, and settings within the larger stream reach. They can occur as migrating features in straight channels, as components of meander bends, or as static structures forced by geologic controls, wood jams, or other obstructions. Consequently, the rates at which velocity or τ increase with discharge at individual riffles and the discharges at which reversals in those parameters might be observed must also vary.

Herein, we attempt to accommodate spatial variability within and between stream reaches by assessing hydraulic conditions over a range of discharges throughout a 40-mile length of the Trinity River, a gravel-bed stream in Northern California. We address complexity in the spatial and temporal distributions of hydraulic variables by evaluating τ as a function of discharge throughout the active channel area with output from a two-dimensional hydraulic model. We then compare the spatial distribution of areas where τ increases at greater or lesser rates with local channel morphology to identify the dominant factors that contribute to pool-riffle maintenance in different geomorphic settings.

Study Area

Our study area is a 40-mile section of the Trinity River between Lewiston Dam and the North Fork Trinity River (Figure 1). The Trinity is a gravel-bed stream with a regulated flow regime characterized by low summer and winter baseflows of 450 and 300 ft³/s, respectively, and spring flow releases that peak between 1500 and 11000 ft³/s (Gaeuman 2014). Tributary inflows during the wet winter months become increasingly important with distance from the dam, such that, in the most downstream reaches, discharges of 1000 ft³/s are equaled or exceeded about half the time during January through March. We chose 8500 ft³/s, which approximates the median annual instantaneous peak flow in the central part of the study, including tributary accretions, to represent the channel-forming discharge throughout. Reach-averaged channel widths range from about 160 ft near the dam to about 120 ft in the more downstream reaches, and reach-averaged channel slopes are near 0.0023 throughout. More than a decade of annual bedload sampling shows that gravel in the Trinity River is transported at relatively low rates when discharge is 4500 ft³/s (Gaeuman et al. 2017). We therefore choose 4000 ft³/s as the approximate threshold of bedload entrainment.
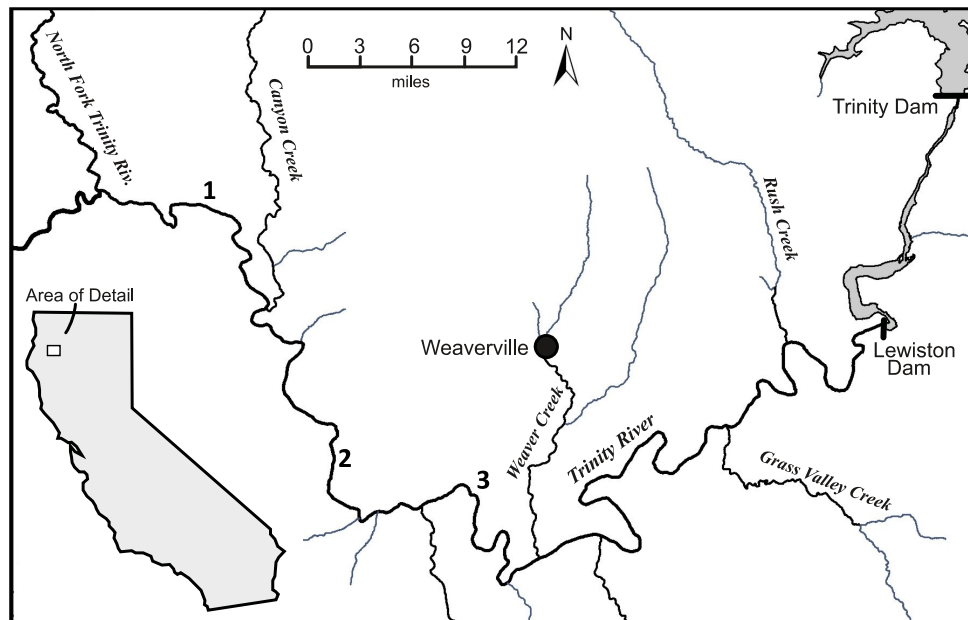

Figure 1. Map showing study area location. Locations of detail sites 1-3 indicated.

Methods

Hydraulic Model

Hydraulic outputs were obtained from SRH-2D (Lai 2010), a two-dimensional hydraulic model developed at the Bureau of Reclamation's Technical Services Center (TSC). The particular implementation of SRH-2D used in this study was created and calibrated under contract with the TSC (Bradley 2018). This model implementation spans the full 40-miles study area and represents conditions in the river at the end of water year 2016. The portion of the computational mesh within the active channel area evaluated in this study consists of about 700,000 individual elements ranging from 20 to about 100 ft^2 in area, with the smallest elements being located near the channel margins. Model outputs include τ in addition to several other standard hydraulic variables such as flow depth, depth-averaged flow velocity, and Froude number.

Model runs are available for 22 discharges ranging from 150 ft^3/s to extreme flood magnitudes that vary with distance from the dam, but for this study we consider only five discharges. Three of them (4000, 6000, 8500, and 11000 ft^3/s) span an interval from approximately the threshold of bedload entrainment to approximately a 5-year recurrence event. We also make use of model outputs for 900 ft^3/s, a relatively frequent discharge that nonetheless inundates most of the active bed area, to represent near baseflow hydraulic conditions across the full channel width.

Data Analysis

The first step for our analyses was to import SRH-2d model outputs along with the computational mesh into ArcMap. We defined the analysis domain as the wetted area at 900 ft^3/s after removing partially-connected side channels and other edge elements with depths less than 0.5 ft and areas less than 20 ft^2. Edge elements with assigned Manning's n values $\geq$ 0.06, indicating the presence of dense riparian vegetation, were also removed. After clipping model outputs to the domain extents, we used database queries to identify the flood discharge (Q) at which individual mesh elements attain maximum τ. Each instance of maximum τ attained at $Q < 11000$ ft^3/s indicates a τ reversals, i.e., a decrease in τ with increasing Q. We then generated polygons designating regions with reversals and the Q associated with the maximum τ.

It is important to recognize that this definition of "reversal" is strict, in the sense that it excludes instances in which the reversal is not maintained over the full range of Q. A decrease in τ when Q increases from 4000 to 6000 ft^3/s, for example, will be recognized as a reversal only if τ at 4000 ft^3/s also exceeds τ at both 8500 and 11000 ft^3/s. Instances in which τ decreases relative to the next larger Q but is eventually exceeded by τ at an even larger Q are not recognized. Thus, our definition of reversals underestimates the frequency of "intermittent" reversals that persist over a narrower range of Q.

To objectively identify geomorphic features within the active stream channel, we classified the 900 ft^3/s hydraulic model output into seven bins according to Froude number, where class boundaries were defined at F_b = 0.1, 0.25, 0.35, 0.5, 0.7, and 0.9, and F_b denotes Froude number at 900 ft^3/s. We then applied database queries to extract the areal extents of regions with maximum τ at each Q within each F_b bin. A preliminary assessment suggested that values of $F_b <$ 0.25 correspond roughly to pool locations and areas with $F_b > 0.5$ correspond roughly to riffles, in general agreement with the findings of Jowett (1993). We generated a polygon shapefile designating regions of pool-like and riffle-like character according to those values of F_b. We

removed polygons less than 1200 ft² in area, as most of these relatively small polygons appear as narrow bands along the channel margins where the hydraulics are influenced by interactions with the banks.

Finally, we overlaid the polygons designating the Q corresponding to maximum τ with the polygons depicting the spatial distribution of F_b bins to produce a polygon shapefile attributed with one of four permutations: $F_b < 0.25$ with reversal, $F_b < 0.25$ without reversal, $F_b > 0.5$ with reversal, and $F_b > 0.5$ without reversal. We removed sliver polygons with areas less than 50 ft² for the sake of simplicity.

Results

Relation of Froude Bins to Pool-Riffle Morphology

About 39% of the stream bed area analyzed displays $F_b < 0.25$, indicating pool-like character, with three-quarters of that area (31%) falling in the 0.1 to 0.25 class (Figure 2). Riffle-like areas with $F_b > 0.5$ constitute about 17% of the total bed area, with about two-thirds of the riffle-like area falling in the 0.5 to 0.7 class. Intermediate values of F_b account for the remaining 43% of the bed area. Visual assessment suggests that this Froude criteria is reasonably effective for identifying the locations of pools and riffles within the active channel bed area (Figure 3). Higher-elevation bars that remain emergent at 900 ft³/s, however, cannot be identified, as the Froude number at zero depth is undefined.
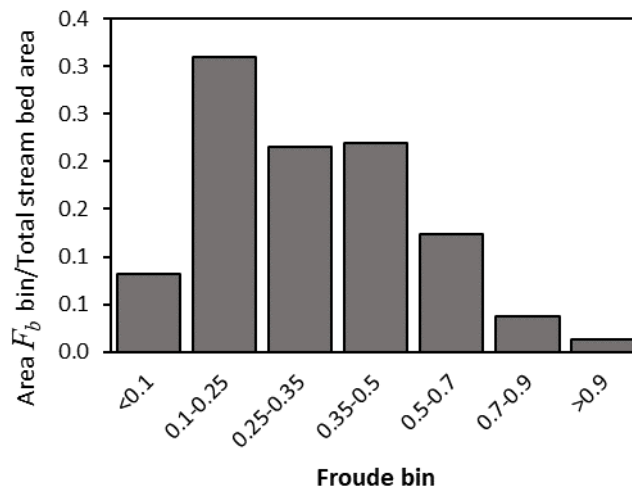

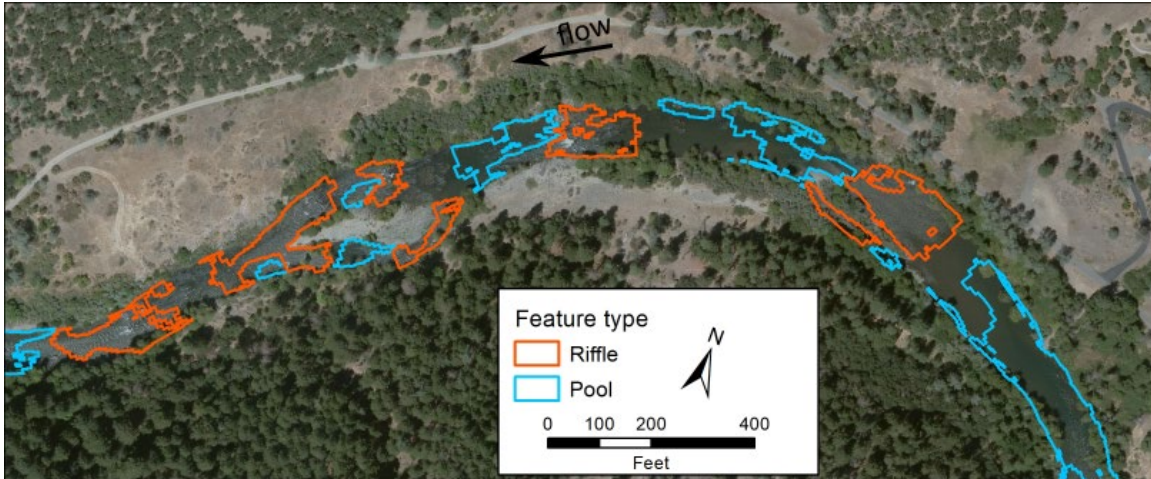**Figure 2.** Proportion of the total stream bed area within each F_b bin.

Figure 3. Example of pool and riffle detection based on F_b.

Reversal Area by Froude Class

It is convenient at this point to introduce some symbology and to clarify some terminology. F_i denotes F_b bin i, where the index i ranges from 1 to 7 and $F_1 < 0.1$. A_{Fi} therefore denotes the stream bed area within F_i. A_{Qji} is defined as the stream bed area within F_i that attains maximum τ at discharge Q_j, where the index j ranges from 1 to 4 and $Q_1 = 4000$ ft³/s. Although τ reversals are defined by attaining τ maximum at any value of $Q < 11000$ ft³/s, the reversals themselves are observed only at the next larger Q, e.g., a τ maximum reaches at Q_1 corresponds to a reversal at Q_2.

For clarity, we point out that the above definition of a hydraulic reversal differs from that implied by Keller (1971) and others who have investigated reversal hypotheses. Most literature on the subject has used the term to describe a reordering of the relative magnitudes of the velocity or τ between riffle and pool locations, regardless of whether the hydraulic variable of interest increases or decreases with increasing discharge at either location. As defined herein, a decrease in τ with increasing discharge at a particular location is considered a reversal regardless of how τ at that location compares to τ at any other location.

The proportion of area over which maximum τ occurs at $Q \leq 8500$ ft³/s (i.e., a τ reversal occurs at some $Q \leq 11000$ ft³/s) ranges from 46 to 81%, with larger percentages corresponding to larger values of F_b (Figure 4a). Integrated over all F_b, fully 54% of the active stream bed experiences a τ reversal at some Q. The areas of reversal, however, are dominated by reversals that occur after a maximum τ is achieved at Q_3 (8500 ft³/s), which approximates a bankfull event throughout most of the study area. In other words, a large proportion of the reversals in all F_b bins (73%) appear at 11000 ft³/s. If only the τ maxima at Q_1 and Q_2 are considered, thereby removing reversals appearing at 11000 ft³/s from consideration, the proportions of bed area that display reversals decline drastically, especially for small F_b, and the smallest, rather than the largest, values of Q_j accounts for the largest share of the remaining reversal area.

For pool-like bins ($F_b < 0.25$), τ reversals at Q_2 or Q_3 (i.e. maximum τ at Q_1 or Q_2) occur over just 5% of the stream bed area assigned to those bins. The proportions of area with reversals at Q_2 or Q_3, however, increase monotonically with increasing F_b, reaching 35% for F_5 and peaking at 55% for F_7. Across all riffle-like areas, as defined according to $F_b > 0.5$, the overall percentage of areas

with reversals at Q_2 or Q_3 is 39%, a figure that is only modestly larger than the value for the F_5 bin alone because less than a third of the combined area has $F_b > 0.7$. The proportions of all Q_2 or Q_3 reversals that occur at Q_2 also increase substantially with increasing F_b – from a value of 33% for F_1, that proportion increases to 70% for F_5 and to 91% for F_7 (Figure 4a). Across all $F_b > 0.5$, 76% of Q_2 or Q_3 reversals are observed at Q_2, indicating that, in riffle-like environments, maximum values of τ are frequently attained near the threshold of entrainment.

The proportions of areas with reversals at Q_2 or Q_3 are smaller and distributed more symmetrically with respect to F_b when expressed as proportions of total bed area (Figure 4b). At 4.2%, F_5 accounts for the largest area of Q_2 or Q_3 reversals relative to the total stream bed area, but F_4 is close behind at 3.9% due to its larger size, which is 77% greater in total area than F_5. Riffle-like areas ($F_b > 0.5$) with Q_2 or Q_3 reversals accounts for 6.7% of the total bed area and 45% of all such reversals, even though those F_b bins occupy only 17% of the active stream bed. Conversely, pool-like areas (F_1 and F_2) with reversals at Q_2 or Q_3 account for only 2.1% of the total bed area and 14% of such reversals, despite comprising nearly 40% of the total bed.
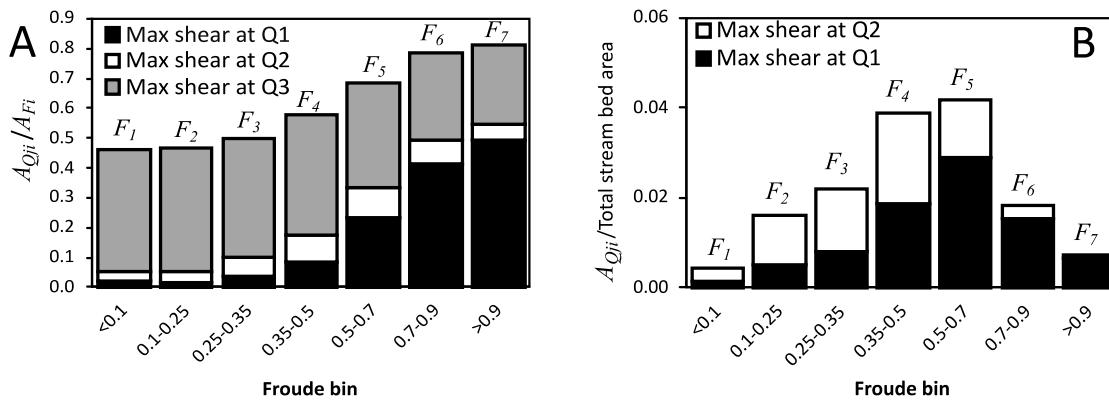

Figure 4. A) Proportion of the total stream bed area within each F_b bin (A_{Fi}); B) Ratio of the areas of τ maxima attained at each $Q_j \leq 8500$ ft^3/s in each F_b bin (A_{Qji}) to A_{Fi}.

Persistence of Reversals

Because the definition of reversals adopted for this study identifies only persistent reversals, it is possible that the hydraulic model results contain many unidentified intermittent reversals, in which τ decreases as Q_j goes to Q_{j+1} only to increase to a new maximum as Q continues to increase. We evaluated this possibility by identifying the Q associated with maximum τ with 11000 ft^3/s excluded.

When only $Q \leq 8500$ ft^3/s are considered, τ maxima at 8500 ft^3/s occurs over about 85% of the bed area, whereas maxima at 4000 and 6000 ft^3/s occur over about 8.8 and 6.9% of the area, respectively (Figure 5). When τ at 11000 ft^3/s is included in the assignment of maxima, more than half the maxima assigned to 8500 ft^3/s is transferred to 11000 ft^3/s. Inclusion of the larger Q, however, has very little effect on the proportion of area assigned to maxima at the two smallest discharges, which hold nearly steady at 8.4 and 6.5%, respectively. Thus, not only are instances of intermittent reversals relatively rare over the range of Q considered, but these results clearly demonstrate that τ reversals tend to be persistent over Q. Even for τ reversals initiated near the

threshold of gravel entrainment, at least 93% of the reversed area is maintained through events well beyond the bankfull flood.
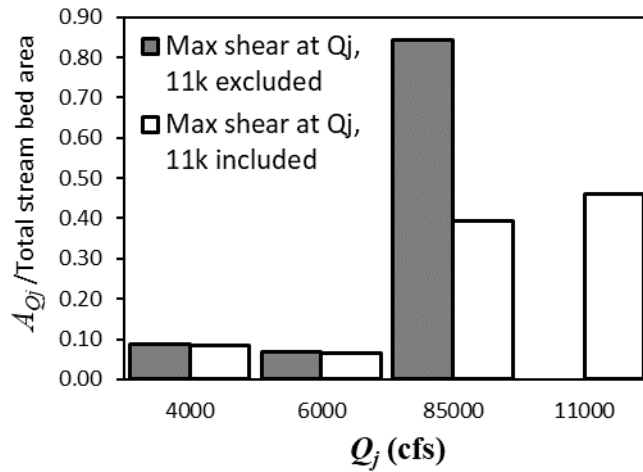

Figure 5. Proportions of total stream bed area with maximum τ at Q_j, where the Q of maximum τ is calculated with τ values for 11000 ft³/s included and with τ values for 11000 ft³/s excluded.

Detail Site Characteristics

The statistical results presented above identify to some extent how τ reversals are distributed on the landscape and over a range of relatively frequent flood discharges, but they shed little light on the mechanisms that govern their occurrence. We now consider a selection of pool-riffle sequences drawn from our Trinity River study area in greater detail to evaluate the mechanisms that determine where and when reversals occur and how they relate to the locations of riffles and pools and other aspects of stream morphology. The detail sites presented were chosen to represent a range of physical configurations, as well as to emphasize similarities across sites. Their locations are indicated on Figure 1.

Figure 6 depicts a typical configuration where a long riffle defined by F_b > 0.5 lies between two adjacent pools, as defined by F_b < 0.25. Open polygons outlined in black in the top image indicate riffle areas that exhibit τ reversals at Q ≤ 8500 ft³/s, whereas open polygons outlined in blue indicate pool areas where reversals at Q ≤ 8500 are absent. At this site, reversal was evident at 6000 ft³/s (maximum τ at 4000 ft³/s) throughout the open black polygon. A small polygon outlined in black and filled with black stipples denotes an area classified as a riffle area where τ continues to increase through 8500 ft³/s, and a small polygon outlined in blue with blue stipples indicates an area classified as a pool where reversal does occur at Q ≤ 8500 ft³/s. Riffle areas where reversals occur only at 11000 ft³/s are neglected on all detail site photomaps to avoid overcomplicating the figures.

The area-weighted average value of τ within each of the four polygon types found at detail site 1 – riffle or pool with or without reversal at Q ≤ 8500 ft³/s – are plotted against Q in the lefthand panel of Figure 7. Error bars shown for the riffle curve are equal to 1 standard deviation. Standard deviations for the other curves are neglected to minimize clutter but are of similar magnitude. Mean τ within the riffle polygon decreases steadily with Q from approximately 1 lbs/ft² at 4000

ft³/s to about 0.65 lbs/ft² at 8500 ft³/s, and reach a minimum of about 0.57 lbs/ft² at 11000 ft³/s. Meanwhile, mean τ within the pool polygon increases steadily with Q from less than 0.4 lbs/ft² at 4000 ft³/s to approximately match τ at the riffle at 8500 ft³/s and slightly exceed τ at the riffle at 11000 ft³/s. The mechanism of reversal over most of the riffle area and the lack of reversal through most of the pool area is evident in the bottom panel of Figure 6, which shows the modeled flow velocity field at 11000 ft³/s with all polygons outlined in black and with stippling removed to maximum visibility against the background colors.
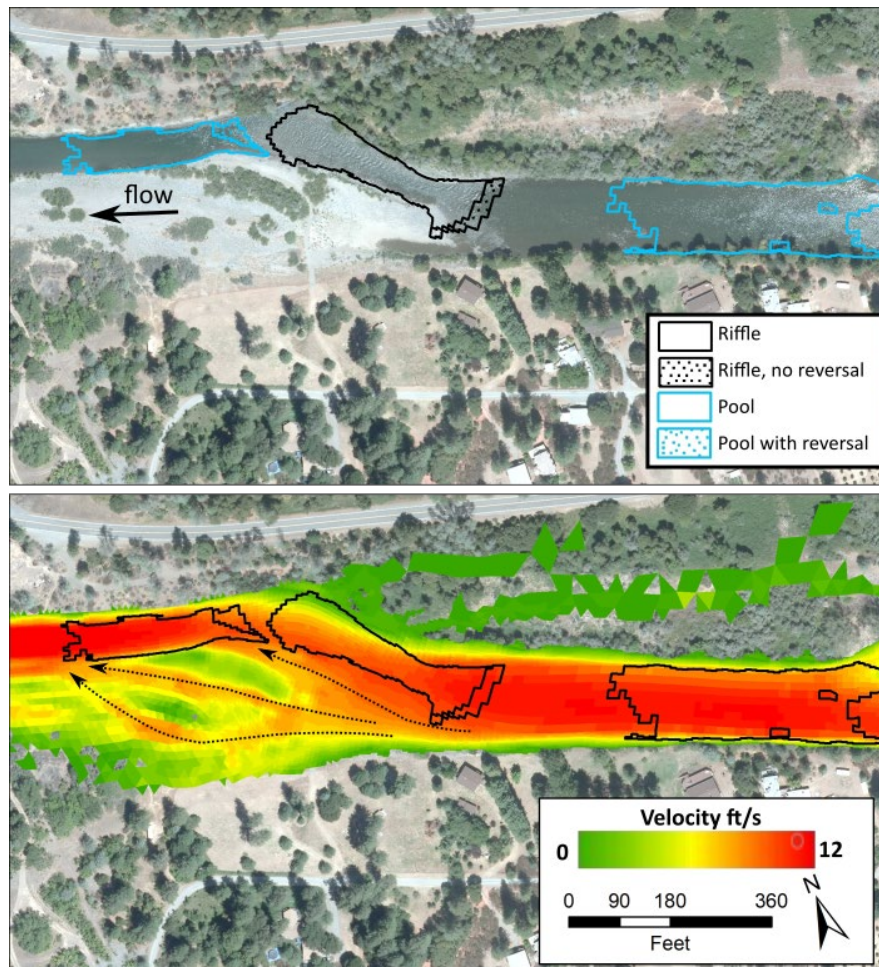

Figure 6. Detail site 1 at summer baseflow discharge (top) and overlain with modeled flow velocity field at 11000 ft³/s (bottom).

At small Q, flow is confined to approximately the wetted extents shown in the upper panel of the figure. As Q increases, however, a progressively larger proportion of the flow is conveyed over the left overbank area (lower panel, Figure 6). The dotted arrows highlight the primary overbank flow paths evident at 11000 ft³/s. It is apparent that the riffle is located where flow diverges from the baseflow channel and the width over which water is conveyed approaches a maximum. The pools, on the other hand, are located where flow is confined to the baseflow channel area or converges toward an anomalously narrow section of channel. Although τ fails to reverse in a small area at the upstream end of the riffle, it remains nearly constant over the full range of Q. Conversely, the small roughly triangular region at the upstream end of the downstream pool where reversal does

occur is located to the right of the main core of downstream flow at 11000 ft³/s, which is displaced away from the concave right bank.
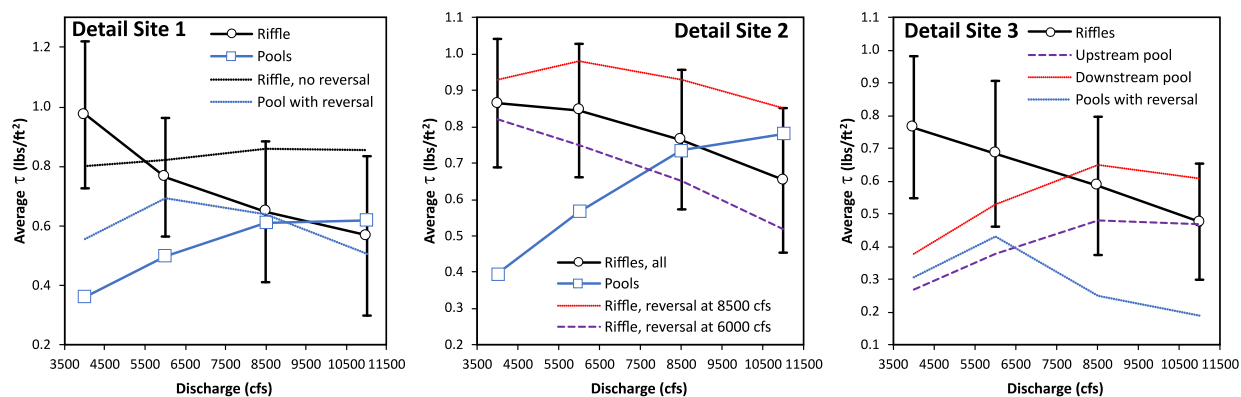

Figure 7. Average values of τ within riffle and pool polygons at detail sites, as described in the text.

A similar configuration exists at detail site 2, except that different portions of the riffle area at site 2 undergo reversal at different discharges (Figure 8). Reversals in the open black polygon in the upper panel of Figure 8 are evident at 6000 ft³/s, whereas reversals in the cross-hatched polygon become evident at 8500 ft³/s. No pool areas exhibit reversals at this site, and riffle areas that fail to reverse are sufficiently small that they are ignored. As shown in the middle panel of Figure 7, τ averaged over both riffle polygons exhibits a steady decrease with increasing Q, although the decrease from 4000 to 6000 ft³/s is relatively small. Meanwhile, τ averaged over both pool polygons increase substantially over the range of modeled Q, reaching a maximum at 11000 ft³/s that is 20% larger than τ averaged over the riffle.

As is the case at detail site 1, the riffle at detail site 2 is located where flow diverges from the baseflow channel and is increasingly conveyed across the left overbank area as Q increases. Also as in site 1, the wider overbank flow is associated with a slight curve in the baseflow channel, such that the core of the downstream flow becomes straighter as Q increases. As the streamlines straighten, they no longer conform to the curvature of the baseflow channel, and downstream conveyance is displaced away from the concave right bank. Flow velocities and τ therefore begin to decrease near the right bank first, and the region over which the decreases are observed expands toward the convex bank as Q continues to increase. This dynamic is particularly clear at site 2, as reversal in the open riffle polygon on the right side of the channel is evident at 6000 ft³/s, whereas reversal in the cross-hatched riffle polygon is delayed to a larger Q and values of τ are 30 to 40% larger over the full range of Q (Figure 7).

A more pronounced lateral shift in the location of greatest downstream conveyance appears to be the primary driver of τ reversals at detail site 3, where a mid-channel bar bifurcates flow into two separate anabranches. At baseflow, the left anabranch conveys the majority of the discharge though a nearly 90-degree bend with a pool at its apex (Figure 9). At large Q, however, the majority of the flow follows a straighter path to the right of the mid-channel bar. The core of the downstream flow enters the right anabranch at its upstream end, but midway through the bifurcation the high velocity core abandons the baseflow alignment and instead passes through the right overbank area. As a result, τ reversals are widespread throughout the left anabranch, including in the two pools shown with blue stippling in the left panel of Figure 9 and represented

by the blue dashed curve in Figure 7. Mean τ in the three riffle areas decrease steadily from a maximum at 4000 ft³/s, whereas the area within the two nearby pools with reversals attain maximum τ at 6000 ft³/s. This delay in maximum τ in the left anabranch suggests that most of the stream flow continues to be conveyed through the left anabranch at 6000 ft³/s, and then shifts abruptly to the right anabranch prior to Q reaching 8500 ft³/s.
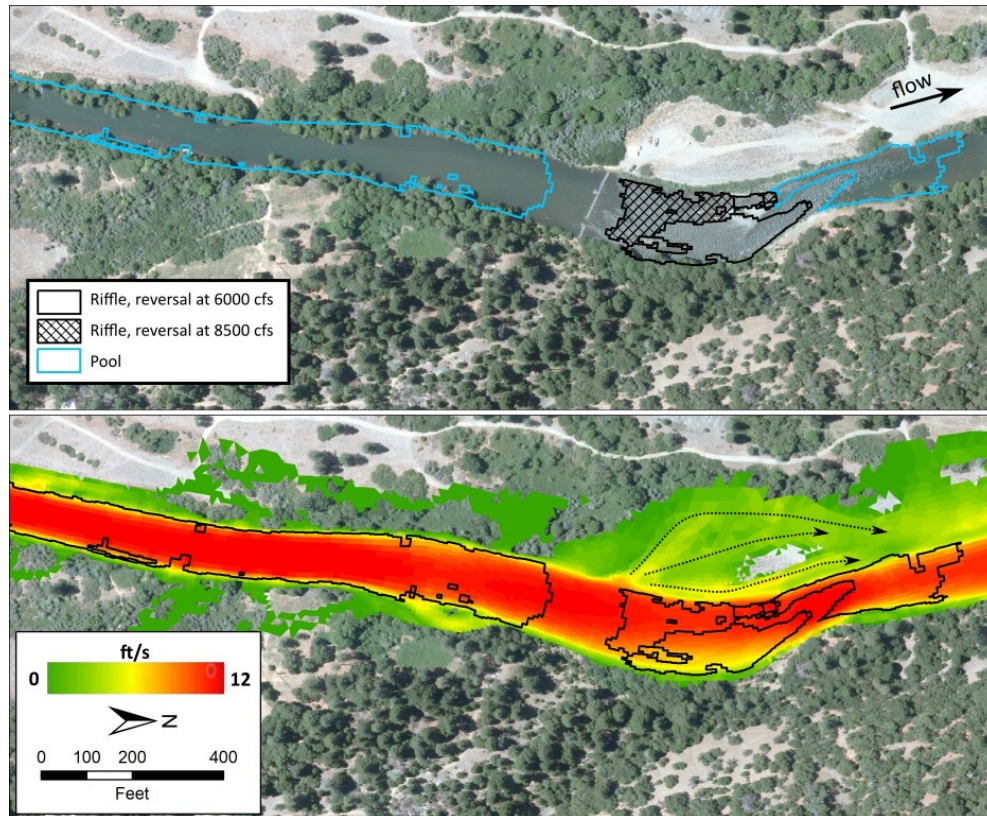

Figure 8. Detail site 2 at summer baseflow discharge (top) and overlain with modeled flow velocity field at 11000 ft³/s (bottom).

The two other pools at site 3, located upstream and downstream from the mid-channel bar, lack reversals at $Q \leq 8500$ ft³/s. The large pool at the downstream end of the site reaches a maximum τ at 8500 ft³/s before declining slightly to a value at 11000 ft³/s that is nonetheless 28% larger than τ at the riffles. The large pool upstream from the mid-channel bar also displays a general increase in τ with increasing Q and, at 11000 ft³/s, reaches a level commensurate with τ at the riffles. Mean τ in that pool, however, is about 25% smaller across all flows than in the downstream pool, suggesting that the mid-channel bar represents an effective hydraulic control that generates backwater conditions in the pool at large Q. Such a backwater effect would be consistent with the abrupt shift in flow conveyance from the left to the right anabranch as Q approaches 8500 ft³/s noted above.
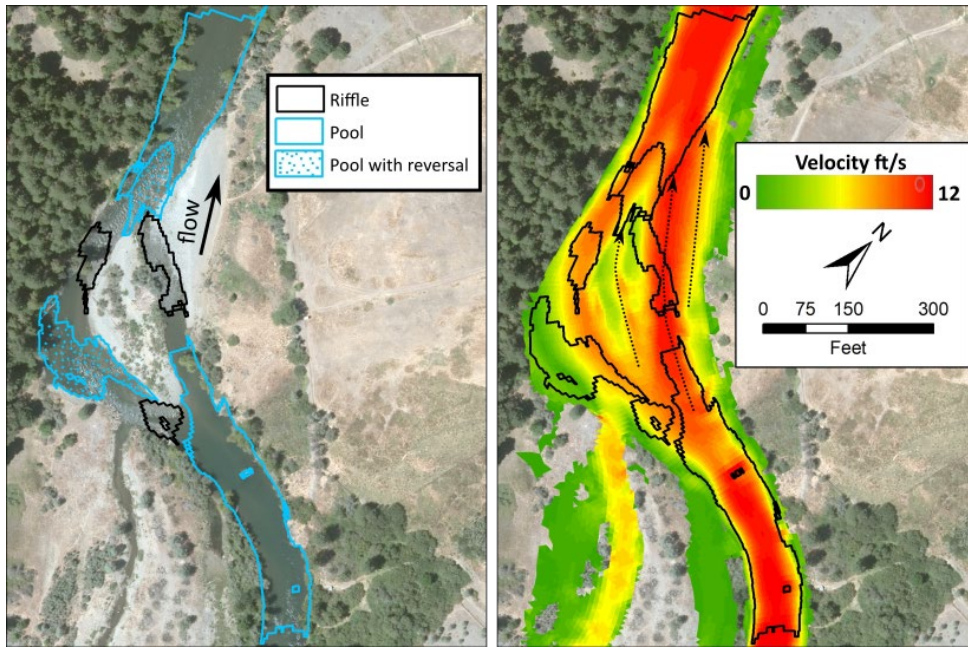
Figure 9. Detail site 3 at summer baseflow discharge (top) and overlain with modeled flow velocity field at 11000 ft^3/s (bottom).

Discussion

As can be seen in Figure 7, the point reversals described above frequently result in "relative reversals," i.e., the average magnitude of τ is greater in pool areas than in nearby riffle areas, when Q becomes large. The same figures, however, also make it clear that τ magnitudes in many other pools remain smaller than τ in nearby riffles over the full range of Q. The same is true of average values of τ computed over the entire study area, which for areas classified as riffles are 1.45 to 2.38 times greater than the averages for areas classified as pools (Figure 10). Variability about those averages is large, however, so that for $Q \geq 8500$ ft^3/s the mean τ for riffles is within one standard deviation of the mean τ for pools.

Although point τ reversal occurs over less than half of the riffle area, increases in τ with increasing Q in riffle areas that do not reverse are typically small. The generally slow rate of change in τ at riffles is evident in the riffle curve in Figure 10, which is virtually flat across the range of discharge. In other words, riffles tend to exist in areas where τ is relatively constant with respect to discharge. Areas classified as pools show steeper rates of increase in τ as discharge increases beyond 4000 ft^3/s, but the maximum average value attained at 11000 ft^3/s is just 0.56 lbs/ft^2 (Figure 10). Assuming a Shields parameter of 0.03 and a median particle size of 60 mm, that magnitude of τ is insufficient to entrain the large gravel and small cobble typical of the substrate framework in the Trinity River. So, although the τ reversals described thus far can perhaps account for coarse sediment deposition at riffles during floods, the lack of reversals in pools does not account for the scour at large Q that is presumably necessary for the creation and maintenance of pools.
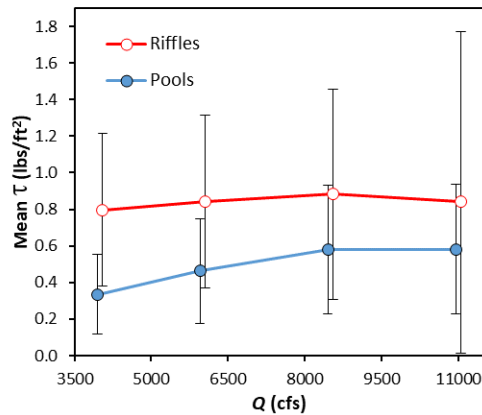
Figure 10. Mean τ within all pools and all riffles for $Q \geq 4000$ ft³/s. Error bars are one standard deviation.

Where point reversals in τ are detected, they appear to be driven primarily by flow divergence in local areas where the fastest, most forceful flow is displaced laterally away from the reversal area. Although this is most commonly observed at riffles, it can also occur at pools, such as at the pool at the apex of the left anabranch of detail site 3. At that location, the core of high velocity flow is displaced at large Q to the right of the mid-channel bar, well away from the apex pool. One could perhaps speculate that bedload bypasses the apex pool at all Q large enough to deliver coarse bedload, such that coarse materials never reach it. An argument along those lines, however, cannot account for maintenance of the large pool at the upstream end of the site where the mean τ never exceeds 0.48 (Figure 7) and the high-velocity core of the flow remains squarely within the low-flow channel (Figure 9). Something important is clearly missing from our analysis.

One possibility is that the hydraulic model used to calculate hydraulic conditions systematically underestimates τ in pools. Measurements in both field (MacVicar and Roy 2007) and laboratory settings (MacVicar and Rennie 2012) show that deceleration of the flow that accompanies the transition to greater depth in pools generates vortices characterized by large velocity fluctuations and Reynolds stresses that greatly exceed time-averaged values of τ. The turbulence generated by the deceleration in the upstream portion of pools includes vertical and lateral velocity components directed downward and toward the center of the flow so that flow convergence occurs even in the absence of any lateral constriction (MacVicar and Rennie 2012). Three-dimensional velocity fluctuations such as these cannot be resolved with a two-dimensional or a time-averaged model.

Conclusions

Froude number calculated for a relatively low reference discharge (F_b) proved to be a reasonably effective metric for classifying regions within the baseflow channel as riffle-like or pool-like. It also proved to be effective for identifying areas where τ is more likely to decrease with increasing discharge, with regions classified are riffles being about 8 times more likely to display τ reversals than regions classified as pools. In addition, regions classified as riffles that lack reversals often experience small rates of increase in τ with increasing discharge so that τ remains almost constant over a wide range of discharge.

Reversals in τ are most frequent after a maximum τ is attained at the approximate bankfull discharge of (8500 ft³/s), with 73% of all reversals first appearing at 11000 ft³/s. If the remaining reversals are considered separately, however, more than half occur after a maximum τ is attained at 4000 ft³/s, which is close to the threshold of gravel entrainment. At least 93% of τ maxima first attained at 4000 and 6000 ft³/s persist as maxima through the full range of discharges.

Riffles and areas where τ reversals occur are located where the wetted area available to convey flood discharge is abnormally wide and flow diverges onto overbank area. As discharge increases and streamlines straighten, the band of highest-velocity flow is displaced laterally and partially decouples from the baseflow channel alignment. Lateral displacements of the main flow tend to occur where the baseflow channel is curved and are especially large where major secondary channels are available.

Point τ reversals in pools are rare. According to our hydraulic model, however, the magnitudes of τ in most pools are nonetheless too small to entrain coarse bedload even at the largest discharges. We therefore cannot account for how pools are created or maintained with the model output at our disposal. We suspect that actual τ in the pools is significantly greater than the modeled τ due to turbulence and large Reynolds stresses generated as the flow decelerates in the transition to greater depths in pools. Such processes cannot be resolved with a time-averaged two-dimensional model.

References

Bradley, D.N. 2018. Trinity River 40 mile hydraulic model: Update with 2016 topography. U.S. Bureau of Reclamation, Technical Services Center, Technical Report No. SRH-2018-11.

Cao, Z., Carling, P., and Oakey, R. 2003. "Flow reversal over a natural pool-riffle sequence: A computational study," Earth Surface Processes and Landforms, 28:689-705, doi:10.1002/esp.466.

Carling, P.A. 1991. "An appraisal of the velocity-reversal hypothesis for stable pool-riffle sequences in the River Severn, England," Earth Surface Processes and Landforms 16:19-31.

Gaeuman, D. 2014. "High-flow gravel injection for constructing designed in-channel features," River Research and Applications, 30(6):685-706, doi:10.1002/rra.2662.

Gaeuman, D., R.L. Stewart, Schmandt, B., and C. Pryor. 2017. "Geomorphic response to gravel augmentation and high-flow dam release in the Trinity River, California," Earth Surface Processes and Landforms, 42:2523-2540, doi:10.1002/esp.4191.

Hawkins, C.P., Kershner, J.L., Bisson, P.A., Bryant, M.D., Decker, L.M., Gregory, S.V., McCullough, D.A., Overton, C.K., Reeves, G.H., Steedman, R.J., and Young, M.K. 1993. "A hierarchical approach to classifying stream habitat features," Fisheries, 18(3):3-10.

Jowett, I.G. 1993. "A method for objectively identifying pool, run, and riffle habitats from physical measurements," New Zealand Journal of Marine and Freshwater Research, 27(2):241-248.

Keller, E.A. 1971. "Areal sorting of bed-load material: the hypothesis of velocity reversal," Geological Society of America Bulletin, 82(3):753-756.

Knighton, D. 1998. Fluvial forms and processes. John Wiley and Sons, New York, 383 pp.

Leopold, L.B., Wolman, M.G., and Miller, J.P. 1964. Fluvial processes in geomorphology. Dover, Mineola, N.Y., 522 pp.

Lisle, T.E. 1979. "A sorting mechanism for a riffle-pool sequence," Geological Society of America Bulletin, 90, 616–617.

MacWilliams, M.L. Jr., Wheaton, J.M., Pasternak, G.B., Street, R.L., and Kitanidis, P.K. 2006. "Flow convergence routing hypothesis for pool-riffle maintenance in alluvial rivers," Water Resources Research, Vol. 42, W10427, doi:10.1029/2005WR004391.

MacVicar, B.J. and Roy, A.G. 2007. "Hydrodynamics of a forced riffle pool in a gravel bed river: 1. Mean velocity and turbulence intensity," Water Resources Research, Vol. 43, W12401, doi:10.1029/2006WR005272.

MacVicar, B.J. and Rennie, C.D. 2012. "Flow and turbulence redistribution in a straight artificial pool," Water Resources Research, Vol. 48, W02503, doi:10.1029/2010WR009374.

Pasternack, G.B, Bounrisavong, M.K., and Parikh, K.K. 2008. "Backwater control on riffle–pool hydraulics, fish habitat quality, and sediment transport regime in gravel-bed rivers," Journal of Hydrology, 357:125– 139, doi:10.1016/j.jhydrol.2008.05.014.

Thompson, D.M. 2010. "The velocity-reversal hypothesis revisited," Progress in Physical Geography, 35(1):123-132.

Wilkinson, S.N., Keller, R.J., and Rutherfurd, I.D. 2004. "Phase-shifts in shear stress as an explanation for the maintenance of pool-riffle sequences," Earth Surface Processes and Landforms, 29:737–753.